Supplementary information

Magnesium-enriched poultry manure enhances phosphorus bioavailability in biochars

Aline do Amaral Leite[1,2]; Leônidas Carrijo Azevedo Melo[1,2]; Luis Carlos Colocho Hurtarte[3]; Lucia Zuin[4]; Cristiano Dela Piccolla[5]; Don Werder[6]; Itamar Shabtai[7]; Johannes Lehmann[2,8,9,*]

[1]Federal University of Lavras/UFLA - Soil Science Dept., 37200-000, Lavras, Brazil.

[2]Soil and Crop Sciences, School of Integrative Plant Science, Cornell University, Ithaca, NY 14850, USA.

[3]European Synchrotron radiation Facility/ESRF – Grenoble, France.

[4]Canadian Light Source/CLS – Saskatoon, Canada.

[5]University of Western Santa Catarina/UNOESC, Brazil.

[6]Cornell Center for Materials Research, Cornell University, Ithaca, NY 14850, USA.

[7]Department of Environmental Science and Forestry, The Connecticut Agricultural. Experiment Station, New Haven, CT, 06511, USA.

[8]Department of Global Development, Cornell University, Ithaca, NY 14850, USA.

[9]Cornell Atkinson Center for Sustainability, Cornell University, Ithaca, NY 14850, USA

[*]Corresponding author: CL273@cornell.edu

Table S1. Total phosphorus, phosphorus extracted by citric acid 2% and formic acid 2% of poultry manure enriched with magnesium sulfate ($MgSO_4$) and magnesium chloride ($MgCl_2$) (means values ± standard deviation; n=3).

Poultry manure enrichment	T (ºC)	Mg/Ca ratio	Total P (g kg^{-1})	Citric acid (g kg^{-1})	Citric acid (% of total P)	Formic acid (g kg^{-1})	Formic acid (% of total P)
$MgSO_4$	70	0.16	10.4 ± 0.2	5.5 ± 0.2	53.3	5.8 ± 0.0	56.3
$MgCl_2$			10.2 ± 0.0	5.4 ± 0.1	53.3	5.9 ± 0.2	58.3
$MgSO_4$	300		19.3 ± 0.7	8.9 ± 0.8	46.3	9.0 ± 0.6	46.5
$MgCl_2$			14.6 ± 0.9	9.5 ± 0.4	65.1	9.5 ± 0.7	65.2
$MgSO_4$	500		18.8 ± 0.4	17.7 ± 0.8	94.1	17.5 ± 0.4	92.8
$MgCl_2$			15.8 ± 0.8	14.4 ± 0.5	90.8	15.1 ± 0.1	95.6

Table S2. Phosphorus extracted by citric acid 2%, formic acid 2% and water as a function of Magnesium hydroxide modified biochars and magnesium and calcium ratios (means values ± standard deviation; n=3).

Mg/Ca ratio	T (°C)	Citric acid (g kg^{-1})	Citric acid (% of total P)	Formic acid (g kg^{-1})	Formic acid (% of total P)	Water (g kg^{-1})	Water (% of total P)
	70	5.0 ± 0.3	43.8	4.9 ± 0.1	44.9	3.8 ± 0.1	35.0
	300	13.6 ± 0.2	69.8	14.4 ± 0.3	73.1	0.7 ± 0.0	3.7
0.08	500	14.9 ± 0.7	70.8	16.5 ± 0.6	76.0	0.4 ± 0.0	1.8
	600	12.7 ± 0.2	55.1	15.8 ± 0.5	67.7	0.6 ± 0.0	2.8
	700	14.5 ± 0.7	63.6	16.6 ± 0.1	70.9	0.5 ± 0.0	2.1
	70	6.7 ± 0.2	60.6	7.0 ± 0.7	60.6	3.1 ± 0.1	27.5
	300	19.4 ± 1.0	93.8	17.9 ± 0.7	90.0	0.8 ± 0.0	3.8
0.10	500	21.1 ± 1.4	87.5	22.0 ± 1.4	91.0	0.2 ± 0.0	1.2
	600	19.6 ± 0.5	78.8	23.2 ± 0.7	92.1	0.2 ± 0.0	0.8
	700	17.9 ± 0.4	66.2	22.8 ± 1.0	83.1	0.0 ± 0.0	<LD
	70	5.9 ± 0.1	53.9	6.0 ± 0.6	50.2	1.5 ± 0.1	14.2
	300	17.6 ± 0.4	89.6	18.6 ± 0.6	94.3	0.4 ± 0.0	1.9
0.12	500	17.7 ± 0.8	74.4	20.5 ± 1.6	85.8	0.1 ± 0.0	0.5
	600	18.7 ± 0.9	81.3	19.5 ± 0.3	86.5	0.0 ± 0.0	0.3
	700	16.0 ± 0.4	61.0	19.1 ± 0.8	74.2	0.0 ± 0.0	<LD
	70	5.0 ± 0.1	45.1	5.7 ± 0.5	52.6	0.5 ± 0.0	5.0
	300	16.7 ± 0.3	94.3	16.8 ± 0.4	95.6	0.2 ± 0.0	0.9
0.16	500	17.1 ± 0.4	77.8	20.4 ± 1.4	89.5	0.0 ± 0.0	0.2
	600	16.1 ± 0.3	75.2	19.6 ± 0.5	90.3	0.0 ± 0.0	<LD
	700	15.5 ± 0.4	62.5	17.3 ± 0.5	68.9	0.0 ± 0.0	<LD
	70	5.7 ± 0.5	61.5	4.9 ± 0.1	56.5	0.4 ± 0.0	5.0
	300	15.2 ± 0.5	91.3	15.0 ± 0.8	89.7	0.0 ± 0.0	0.34
0.20	500	12.4 ± 0.2	70.1	16.7 ± 0.6	95.0	0.0 ± 0.0	<LD
	600	10.6 ± 0.3	54.7	14.7 ± 0.2	72.8	0.0 ± 0.0	<LD
	700	11.5 ± 0.3	57.3	14.7 ± 0.5	73.4	0.0 ± 0.0	<LD

<LD: lower than the detection limit.

Equations to describe the kinetics of P release from poultry manure and biochar (Dang et al., 1994; Shariatmadari et al., 2006):

First order:

$$\ln Q_t = \ln Q_e - k_1 t \qquad \text{eq. 1.}$$

Second order:

$$\frac{1}{Q_t} = \frac{1}{Q_e} + k_2 t \qquad \text{eq. 2.}$$

Elovich:

$$Q_t = \frac{1}{\beta} \ln(a\beta) + (\frac{1}{\beta}) \ln t \qquad \text{eq. 3.}$$

Power function:

$$Q_t = at^b \qquad \text{eq. 4.}$$

Parabolic diffusion

$$Q_t = Q_e + R\, t^{0.5} \qquad \text{eq. 5.}$$

The terms are as follows: Q_t (g P kg^{-1}) is the cumulative P release at t time; Q_e (g P kg^{-1}) is the amount of P release at equilibrium, or maximum P released. Parameters of examined models are listed in Table S3.

The kinetics of P release for unpyrolyzed poultry manure was better fitted to the parabolic diffusion model, with the SE and AIC of 0.36 and 12.8, respectively. However, the power function was better suited for Mg-doped poultry manure, with SE and AIC of 0.32 and 10.7, respectively (Table S3). PM-BC better fitted the parabolic diffusion model, with SE and AIC of 0.33 and 11.2 (HHT of 300 °C), and SE and AIC of 0.057 and -23.8, (HHT of 500 °C). However, best-fitted models of the P release from the Mg-doped poultry manure biochar varied according to the pyrolysis temperature. At HHT of 300°C, P release from Mg-doped poultry manure biochar best fitted the Elovich equation, with SE and AIC of 0.037 and -32.2, respectively, and at HHT of 500°C it best fitted the parabolic diffusion, with SE and AIC of 0.018 and -46.04, respectively (Table S3).

Table S3. Parameters and standard error of estimative (SE) of the examined models for P release kinetics of unmodified and $Mg(OH)_2$-modified poultry manure and biochars.

Models	Parameters	Sample information					
		PM 70 °C	PMB 300 °C	PMB 500 °C	$Mg(OH)_2$ PM 70 °C	$Mg(OH)_2$ 300 °C	$Mg(OH)_2$ 500 °C
Zero Order	Q_e (g P kg^{-1})	5.22	12.49	1.08	4.14	0.40	0.23
	k_1 (h^{-1})	2.40	9.48	0.01	0.03	0.05	0.01
	SE	1.38	1.11	0.14	0.51	0.04	0.04
	AIC	39.75	35.34	-6.32	19.83	-30.60	-29.33
Second Order	Q_e (g P kg^{-1})	5.45	12.70	1.33	4.83	0.44	0.28
	k_2 [(g P $kg^{-1})^{-1}$]	3.32	25.40	0.02	0.04	0.07	0.01
	SE	1.26	1.01	0.13	0.47	0.04	0.04
	AIC	37.91	33.58	-7.10	18.20	32.7	-29.69
Power Function	a (g P kg^{-1} $h^{-1})^b$	3.31	11.41	0.14	0.82	0.10	0.04
	b [(g P $kg^{-1})^{-1}$]	0.14	0.03	0.37	0.32	0.29	0.27
	SE	0.69	0.63	0.08	0.32	0.04	0.03
	AIC	25.81	24.15	-16.89	10.70	-31.77	37.87
Elovich	α (g P kg^{-1} h^{-1})	3.50	11.45	0.20	0.90	0.09	0.06
	β [(g P $kg^{-1})^{-1}$]	-0.55	-0.39	-0.11	-0.56	-0.06	-0.02
	SE	0.82	0.66	0.16	0.56	0.04	0.04
	AIC	29.40	24.91	-3.22	21.91	-32.29	-32.65
Parabolic Diffusion	Q_e (g P kg^{-1})	3.13	11.17	0.12	0.66	0.08	0.04
	R (g P $kg^{-1})^{-0.5}$	0.30	0.22	0.06	0.28	0.03	0.01
	SE	0.36	0.33	0.06	0.37	0.06	0.02
	AIC	12.81	11.19	-23.78	13.36	-24.03	-46.04

k_1: first-order rate constant (h^{-1}); k_2: second-order rate constant [(μg P $g^{-1})^{-1}$]; *a:* (μg P g^{-1} $h^{-1})^b$; *b: desorption* rate coefficient [(μg P $g^{-1})^{-1}$] initial P desorption rate constant (α: initial P desorption rate (μg P g^{-1} h^{-1}); β: P desorption constant [(μg P $g^{-1})^{-1}$]; R: diffusion rate constant; Q_e: amount of P release at equilibrium or maximum P released; SE: standard error of estimative and AIC: Akaike Information Criterion. (Dang et al., 1994; Shariatmadari et al., 2006)

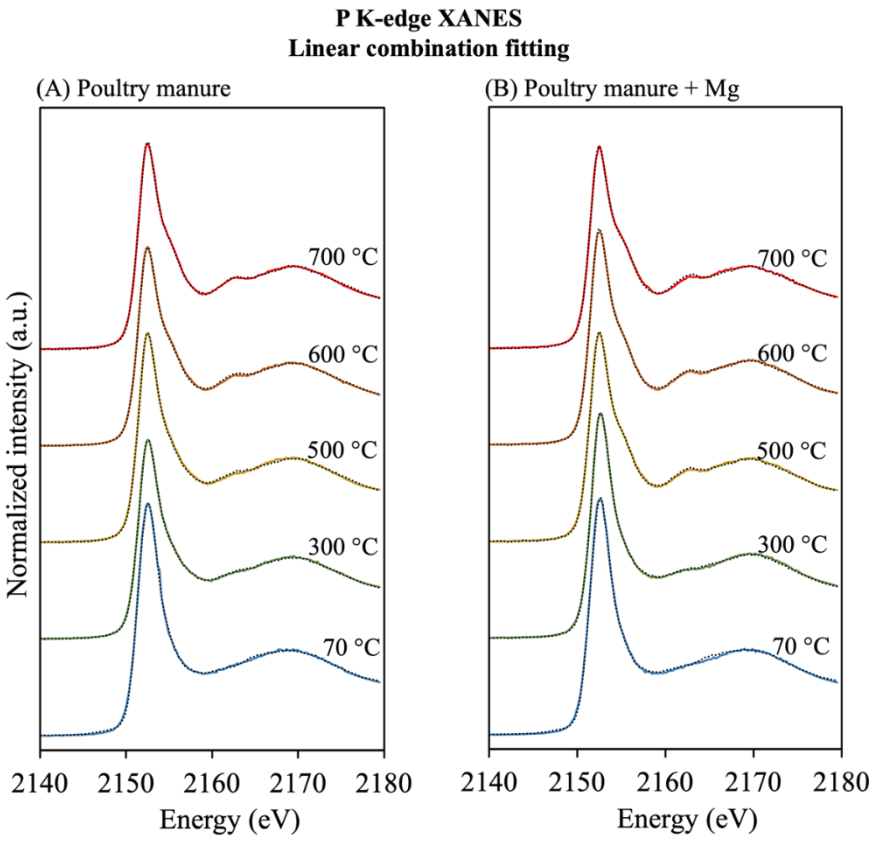

Figure S1. Phosphorus K-edge XANES data and overlaid linear combination fits (dotted lines). Proportions of phosphorus species in the Table 1.

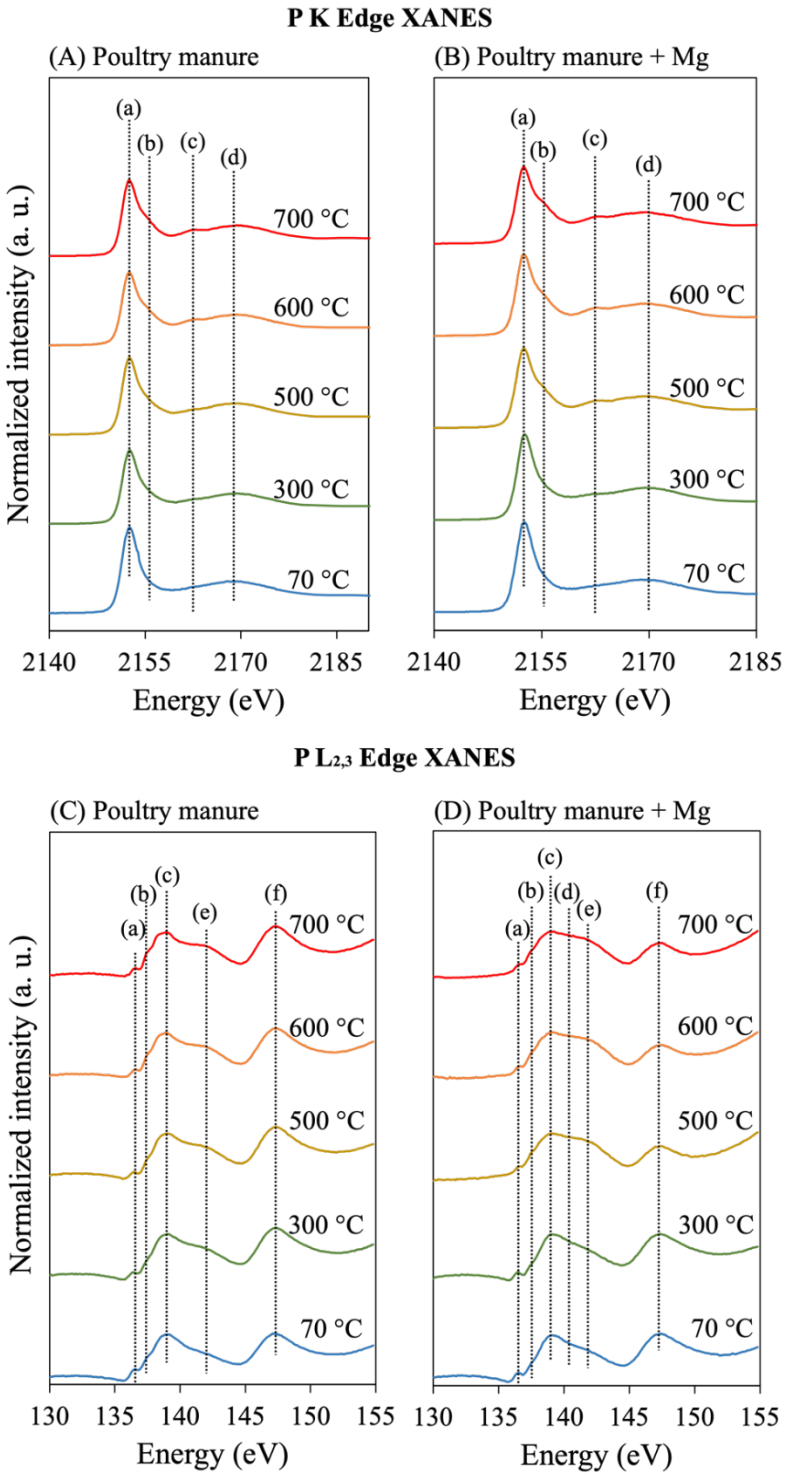

Figure S2. Phosphorus K-edge (A, B) and $L_{2,3}$ edge (C, D) XANES spectra of unmodified (Mg/Ca: 0.08) and $Mg(OH)_2$ added (Mg/Ca: 0.16) poultry manure and biochars. The dotted lines indicate energy levels of spectral features from unique P species. Overlaid linear combination fitting for P K edge in Figure S1. Energy position for $L_{2,3}$ edge in Table S4. Spectra for P compounds in supplementary in Figure S3.

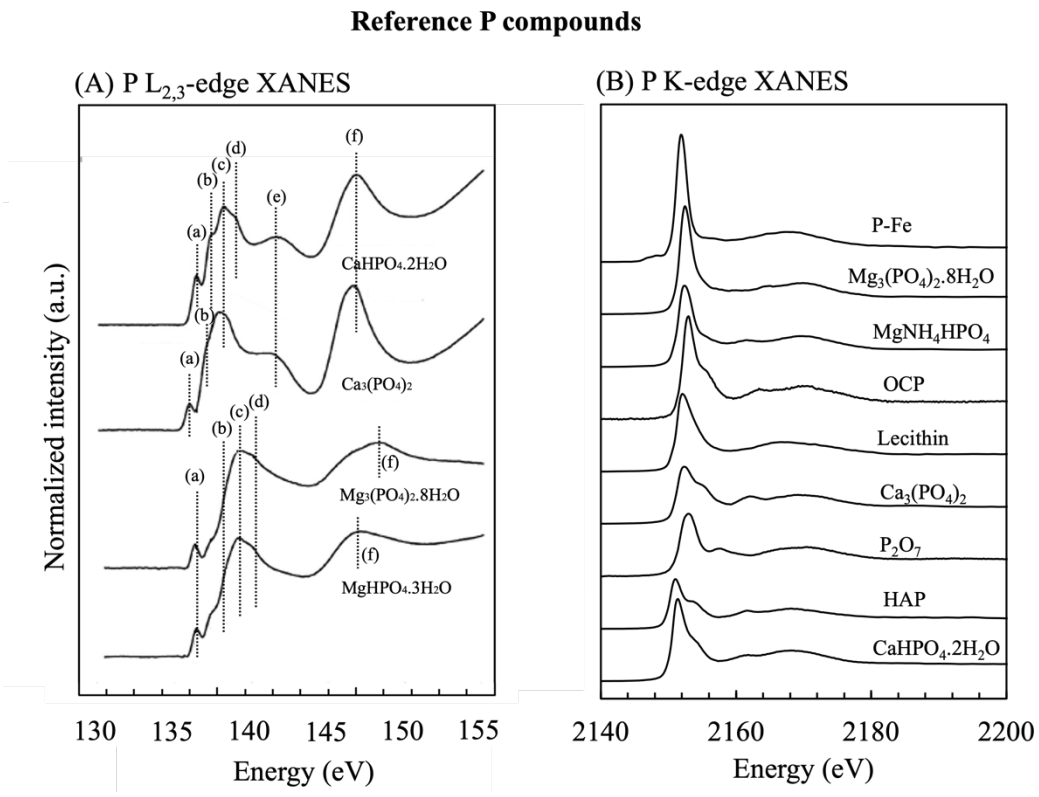

Figure S3. Phosphorus K and $L_{2,3}$-edge XANES spectra for reference phosphorus compounds. (A) The dotted lines indicate energy levels of spectral features from different P species displayed in table S8, Adapted from Kruse et al., 2009. (B) P K-edge XANES spectra for reference compounds adapted from dela Piccolla et al., 2021 and Hesterberg et al., 2017. P-Fe, phosphorus adsorbed on Pahokee peat; OCP, octacalcium phosphate; HAP, Hydroxyapatite.

Table S4. Energy position of P $L_{2,3}$-edge XANES spectra of samples and phosphorus standards (Standards adapted from Kruse et al., 2009).

Samples	Features					
	a	b	c	d	e	f
Poultry manure	136.6	137.3	138.9			147.2
Poultry manure + Mg	136.5	137.4	139.0			147.4
Biochar 300 °C	136.4	137.4	139.0		141.6	147.3
Biochar 300 °C + Mg	136.5	137.4	139.2			147.3
Biochar 500 °C	136.5	137.3	138.9		141.4	147.4
Biochar 500 °C + Mg	136.7	137.4	139.1	139.8	140.8	147.4
Biochar 600 °C	136.6	137.4	138.9		141.8	147.3
Biochar 600 °C + Mg	136.7	137.4	139.1	139.8	141.1	147.5
Biochar 700 °C	136.6	137.4	138.9		141.8	147.4
Biochar 700 °C + Mg	136.6	137.4	139.2	139.9	140.7	147.5

Phosphorus standards	Features					
	a	b	c	d	e	f
$CaHPO_4.2H_2O$	136.4	137.3	138.2	138.9	141.6	146.9
$Ca_3(PO_4)_2$	135.9	136.9	137.9		141.4	146.7
$Mg_3(PO_4)_2.8H_2O$	136.3	138.2	139.2	140.0		148.1
$MgHPO_4.3H_2O$	136.4	138.3	139.1	140.0		147.1

Despite the similarities with K-edge XANES, scanning the absorption from $L_{2,3}$-edge provides more detailed information on species and mineral ordering because of more possible electron transitions and distinguishable features (Kruse et al., 2009; Liu et al., 1992). However, both techniques complement each other. While K-edge provides information on bulk properties of the samples, L-edge, due to its low energy and, thus, lower penetration of the incident beam, is restricted to the surface of the analyzed sample (Bruun et al., 2017).

Table S5. Energy-dispersive spectroscopy (EDS) elemental quantification collected from regions of interest (Figure S4) from poultry manure biochar (Mg/Ca ratio 0.08) and magnesium-modified poultry manure biochar (Mg/Ca ratio 0.16).

PM-BC 300°C: round features elemental quantification

Element	Mass [%]	Mass Norm. [%]	Atomic [%]	abs. error [%] (1 sigma)	rel. error [%] (1 sigma)
Sodium	3.99	3.99	6.35	0.16	4.08
Magnesium	4.97	4.97	7.48	0.18	3.61
Silicon	5.11	5.11	6.66	0.15	2.97
Potassium	31.94	31.94	29.89	0.81	2.54
Calcium	51.25	51.25	46.79	1.34	2.61
Chlorine	2.74	2.74	2.83	0.07	2.71

Mg-PM-BC 300°C: flakes elemental quantification

Element	Mass [%]	Mass Norm. [%]	Atomic [%]	abs. error [%] (1 sigma)	rel. error [%] (1 sigma)
Sodium	6.36	6.36	8.83	0.24	3.72
Magnesium	26.78	26.78	35.15	0.90	3.36
Silicon	2.27	2.27	2.58	0.07	3.27
Phosphorus	4.57	4.57	4.70	0.13	2.95
Chlorine	1.51	1.51	1.36	0.04	2.89
Potassium	39.53	39.53	32.26	1.01	2.56
Calcium	18.99	18.99	15.12	0.51	2.68

Mg-PM-BC 300°C: cubes elemental quantification

Element	Mass [%]	Mass Norm. [%]	Atomic [%]	abs. error [%] (1 sigma)	rel. error [%] (1 sigma)
Sodium	3.73	3.73	5.35	0.14	3.75
Magnesium	22.25	22.25	30.18	0.74	3.31
Phosphorus	2.26	2.26	2.40	0.07	2.92
Chlorine	19.44	19.44	18.07	0.51	2.61
Potassium	46.71	46.71	39.38	1.21	2.60
Calcium	5.61	5.61	4.61	0.16	2.80

Note: Imagens and EDS spectra of nodules, cubes and flakes are shown in Figure S4.

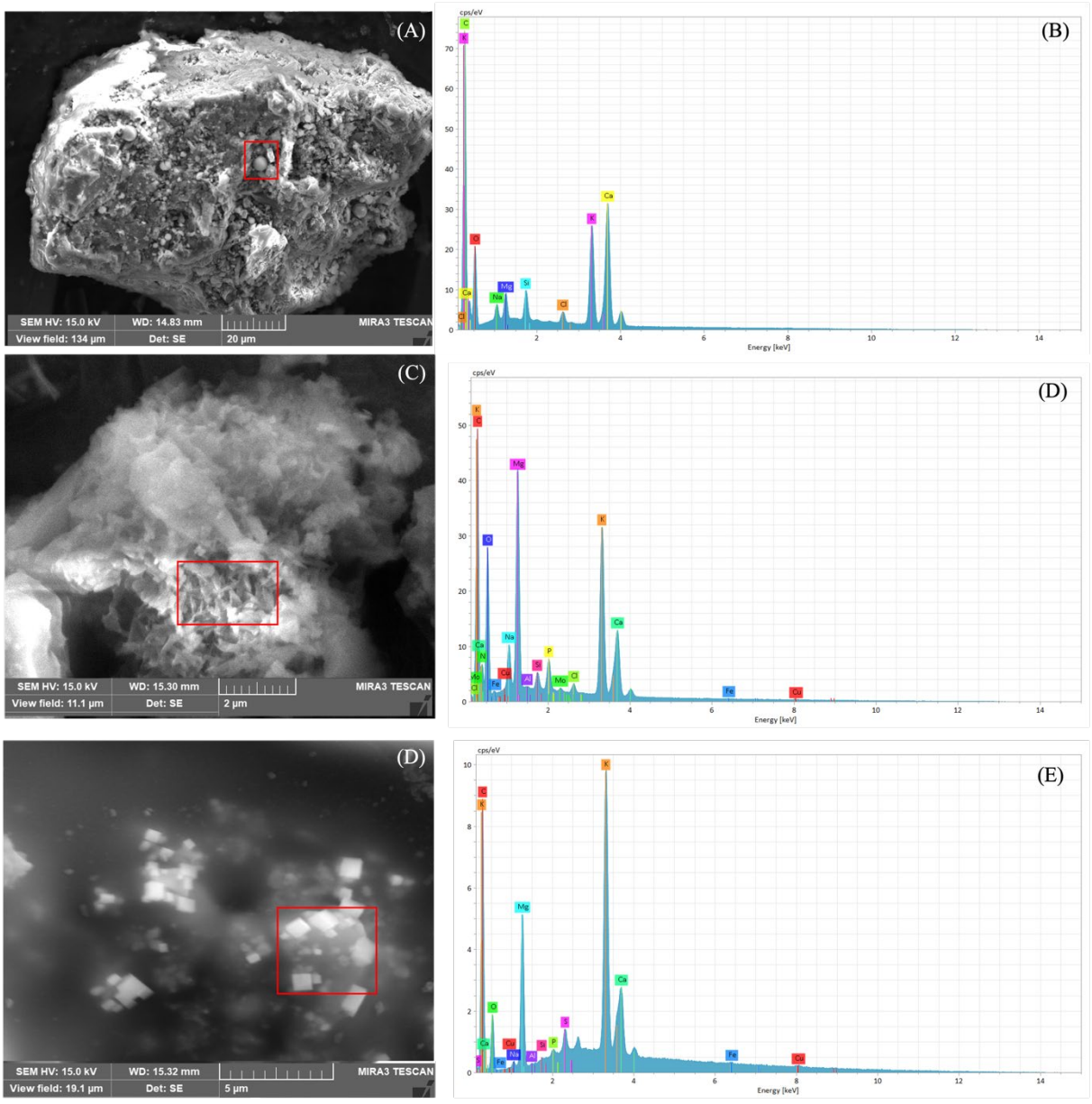

Figure S4. Scanning electron microscopy (SEM) images and Energy dispersive spectroscopy (EDS) spectra of nodules structures of unmodified biochar (Mg/Ca: 0.08) at 300 °C (A and B), and flake and cube structures of $Mg(OH)_2$-modified biochar (Mg/Ca: 0.16) at 300 °C (C, D, E and F).

Table S6. The BET (Brunauer-Emmett-Teller) surface area and total pore volume of raw manure and biochar (Mg/Ca ratio 0.08) and Mg enriched poultry manure and biochar (Mg/Ca ratio 0.16).

Mg/Ca Ratio	T (°C)	BET SA ($m^2\ g^{-1}$)	Total pore volume ($cm^3\ kg^{-1}$)
0.08	70	nonporous	-
	300	low porosity	0.86
	500	3.16 ± 0.04	9.71
	600	2.43 ± 0.05	0.84
	700	nonporous	-
0.20	70	nonporous	-
	300	nonporous	-
	500	nonporous	-
	600	nonporous	-
	700	nonporous	-

The BET surface area analysis (Table S6) indicates that biochar and Mg-biochar possess a non-porous and low-porous morphology. The BET surface area decreased by Mg additions from 3.16 and 2.43 $m^2\ g^{-1}$ to a non-porous condition at 500 °C and 600 °C, respectively. The total pore volume decreased by Mg additions from 9.7 and 0.84 $cm^3\ kg^{-1}$ to undetected at 500 °C and 600 °C, respectively. At both low (300 °C) and high (700 °C) pyrolysis temperatures, biochar and Mg-biochar had low porosity and surface area that did not increase after additions of Mg.

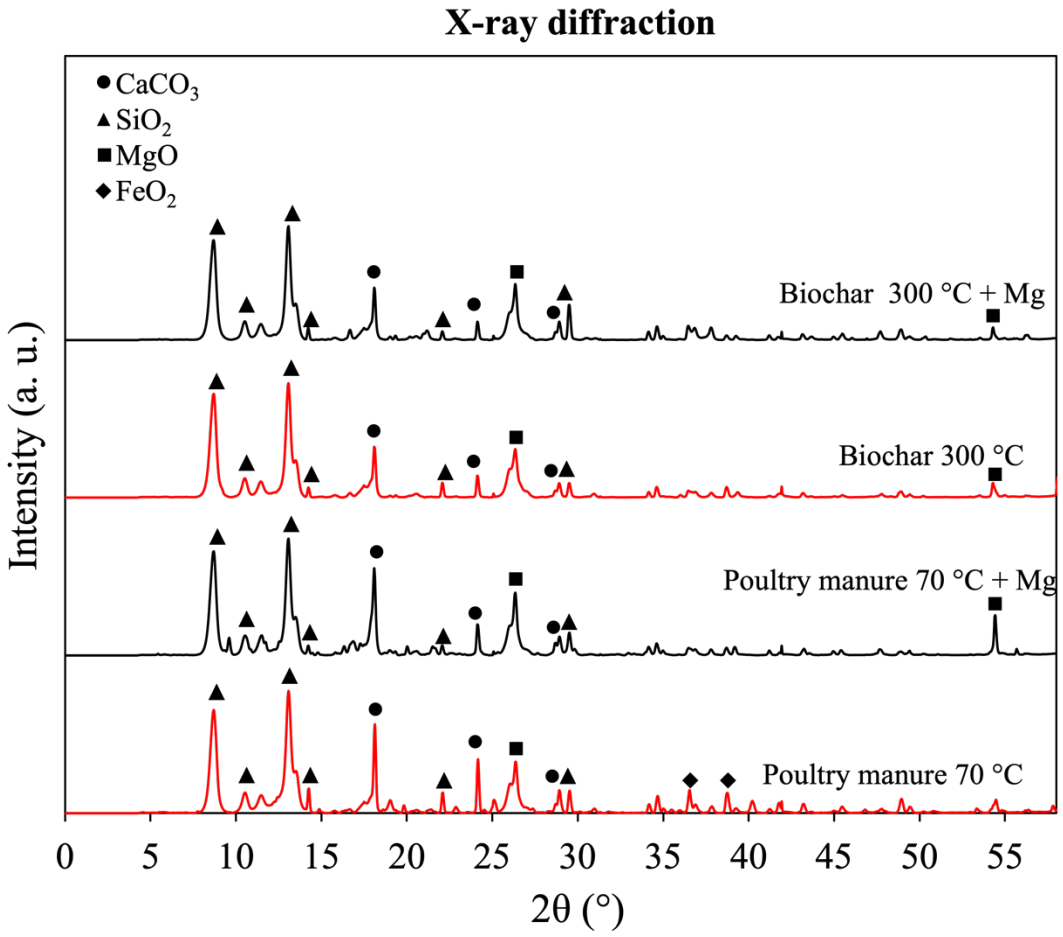

Figure S5. X-ray diffraction of unmodified (Mg/Ca: 0.08) and Mg added (Mg/Ca: 0.16) poultry manure and biochars. XRD peaks position, crystallite size and area under peaks in Table S7.

X-ray diffraction allows the identification of the degree of crystallinity of the samples. Due to the crystallite size of the samples, XRD analyses were carried out at the beamline ID13 of the European Synchrotron Radiation Facility (ESRF). The beamline ID13 is an undulator beamline dedicated to high-lateral-resolution diffraction and scattering experiments using focused monochromatic X-ray beams (Riekel et al., 2010).

Regardless of Mg enrichment, the higher intensities of the crystalline phases for poultry manure and biochar were identified at the following 2θ positions: calcite ($CaCO_3$ – 18 and 24°), cristobalite (SiO_2 – 9 and 13°), and periclase (MgO – 26°), with a d-spacing of 4.89 and 3.68 [Å], 10.1 and 6.77 [Å], and 3.40 [Å], respectively (Figure S5). The crystallite size (in nm) and degree of crystallinity (in %) of unpyrolyzed poultry manure were, on average, 0.27 nm and 57%, which

increased to 0.31 nm and 66% when pyrolyzed (Table S7) (300 °C). After pyrolyzing, the crystallite size of MgO in Mg-doped biochar increased by 25%.

Table S7. Properties of crystalline phases and respectively peak positions of poultry manure and biochars (300 °C).

Crystalline phase	Peak position [°2θ]	PM	Mg-PM	PM-BC	Mg-PM-BC
		Crystallite size [Å]			
SiO_2 – Cristobalite	8.72	188	188	188	188
SiO_2 – Cristobalite	13.06	270	315	315	315
$CaCO_3$ – Calcite	18.10	476	238	317	317
$CaCO_3$ – Calcite	24.15	640	320	320	320
MgO – Periclase	26.21	161	161	120	161
		d-spacing [Å]			
SiO_2 – Cristobalite	8.72	10.15	10.14	10.14	10.14
SiO_2 – Cristobalite	13.06	6.77	6.78	6.78	6.78
$CaCO_3$ – Calcite	18.10	4.89	4.91	4.90	4.90
$CaCO_3$ – Calcite	24.15	3.68	3.68	3.68	3.68
MgO – Periclase	26.21	3.40	3.40	3.40	3.40
		Area under peaks			
SiO_2 – Cristobalite	8.72	15.67	15.93	16.21	15.54
SiO_2 – Cristobalite	13.06	23.01	19.34	18.48	18.82
$CaCO_3$ – Calcite	18.10	7.82	8.98	4.43	4.85
$CaCO_3$ – Calcite	24.15	2.67	1.96	1.17	2.15
MgO – Periclase	26.21	9.50	10.66	9.73	10.00

Note: PM: raw poultry manure; Mg-PM: Mg-modified poultry manure; PM-BC: poultry manure biochar; Mg-PM-BC: Mg-modified poultry manure biochar.

Table S8. Fourier transform infrared spectroscopy (FTIR) spectra band assignments of raw and Mg enriched poultry manure and biochars.

Wavenumber, cm^{-1}	**Band assignment**	**References**
3190, 2914	Aromatic and aliphatic C-H stretching	(Liang et al., 2018; Wang et al., 2014)
1625, 1579	C=O, C=C	(Bekiaris et al., 2016; Farah Nadia et al., 2015)
1407, 1336	C-O stretching, Carbonates, $C-H_2$ bending	(Bekiaris et al., 2016; Domingues et al., 2017; Farah Nadia et al., 2015)
1000, 1026, 1091	P-O Bond, Stretching and bending vibration of Mg-O or Mg-OH	(Bekiaris et al., 2016; Nardis et al., 2021)
873, 794, 754, 705, 615	P-O-P stretching, P-C symmetric, P-O-P, P-O or P=O stretching	(Bekiaris et al., 2016; Li et al., 2016; Nardis et al., 2021)

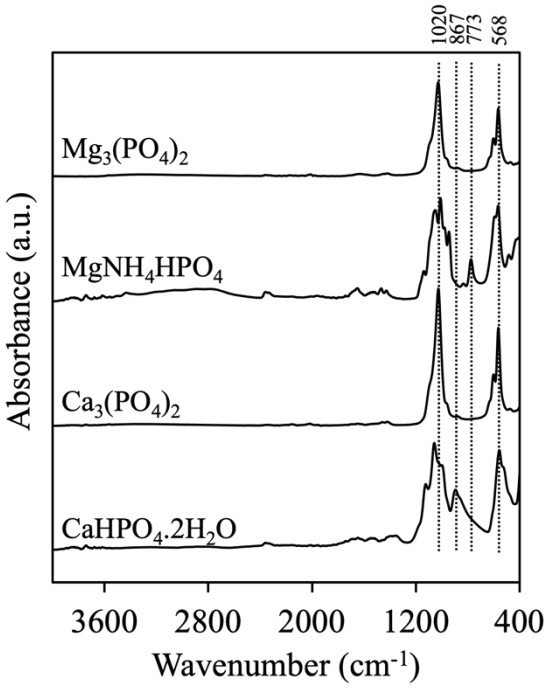

Figure S6. Fourier transform infrared spectroscopy (FTIR) spectra of reference phosphorus compounds.

References

Bekiaris, G., Peltre, C., Jensen, L.S., Bruun, S., 2016. Using FTIR-photoacoustic spectroscopy for phosphorus speciation analysis of biochars. Spectrochim Acta A Mol Biomol Spectrosc 168, 29–36. https://doi.org/10.1016/j.saa.2016.05.049

Bruun, S., Harmer, S.L., Bekiaris, G., Christel, W., Zuin, L., Hu, Y., Jensen, L.S., Lombi, E., 2017. The effect of different pyrolysis temperatures on the speciation and availability in soil of P in biochar produced from the solid fraction of manure. Chemosphere 169, 377–386. https://doi.org/10.1016/j.chemosphere.2016.11.058

Dang, Y.P., Dalal, R.C., Edwards, D.G., Tiller, K.G., 1994. Kinetics of zinc desorption from Vertisols. Soil Science Society of America Journal 58, 1392 – 1399.

dela Piccolla, C., Hesterberg, D., Muraoka, T., Novotny, E.H., 2021. Optimizing pyrolysis conditions for recycling pig bones into phosphate fertilizer. Waste Management 131, 249–257. https://doi.org/10.1016/j.wasman.2021.06.012

Domingues, R.R., Trugilho, P.F., Silva, C.A., de Melo, I.C.N.A., Melo, L.C.A., Magriotis, Z.M., Sánchez-Monedero, M.A., 2017. Properties of biochar derived from wood and high-nutrient biomasses with the aim of agronomic and environmental benefits. PLoS One 12. https://doi.org/10.1371/journal.pone.0176884

Farah Nadia, O., Xiang, L.Y., Lie, L.Y., Chairil Anuar, D., Mohd Afandi, M.P., Azhari Baharuddin, S., 2015. Investigation of physico-chemical properties and microbial community during poultry manure co-composting process. J Environ Sci (China) 28, 81–94. https://doi.org/10.1016/j.jes.2014.07.023

Hesterberg, D., McNulty, I., Thieme, J., 2017. Speciation of Soil Phosphorus Assessed by XANES Spectroscopy at Different Spatial Scales. J Environ Qual 46, 1190–1197. https://doi.org/10.2134/jeq2016.11.0431

Kruse, J., Leinweber, P., Eckhardt, K.U., Godlinski, F., Hu, Y., Zuin, L., 2009. Phosphorus L2,3-edge XANES: Overview of reference compounds. J Synchrotron Radiat 16, 247–259. https://doi.org/10.1107/S0909049509000211

Li, R., Wang, J.J., Zhou, B., Awasthi, M.K., Ali, A., Zhang, Z., Lahori, A.H., Mahar, A., 2016. Recovery of phosphate from aqueous solution by magnesium oxide decorated magnetic biochar and its potential as phosphate-based fertilizer substitute. Bioresour Technol 215, 209–214. https://doi.org/10.1016/j.biortech.2016.02.125

Liang, X., Jin, Y., He, M., Niyungeko, C., Zhang, J., Liu, C., Tian, G., Arai, Y., 2018. Phosphorus speciation and release kinetics of swine manure biochar under various pyrolysis temperatures. Environmental Science and Pollution Research 25, 25780–25788. https://doi.org/10.1007/s11356-017-0640-8

Liu, Z.F., Cutler, J.N., Bancroft, G.M., Tan, K.H., Cave11, 747 R.G., Tse, J.S., 1992. Crystal field 748 splittings of continuum d orbitals. A comparative study on the L2,3 edge X-ray absorption 749 spectra of Si, P and S compounds. Chemical Physics 168, 133-144.

Nardis, B.O., Santana Da Silva Carneiro, J., Souza, I.M.G. de, Barros, R.G. de, Azevedo Melo, L.C., 2021. Phosphorus recovery using magnesium-enriched biochar and its potential use as fertilizer. Arch Agron Soil Sci 67, 1017–1033. https://doi.org/10.1080/03650340.2020.1771699

Riekel, C., Burghammer, M., Davies, R., 2010. Progress in micro- and nano-diffraction at the ESRF ID13 beamline. IOP Conf Ser Mater Sci Eng 14, 012013. https://doi.org/10.1088/1757-899x/14/1/012013

Shariatmadari, H., Shirvani, M., Jafari, A., 2006. Phosphorus release kinetics and availability in calcareous soils of selected arid and semiarid toposequences. Geoderma 132, 261–272. https://doi.org/10.1016/j.geoderma.2005.05.011

Wang, Y., Yin, R., Liu, R., 2014. Characterization of biochar from fast pyrolysis and its effect on chemical properties of the tea garden soil. J Anal Appl Pyrolysis 110, 375–381. https://doi.org/10.1016/j.jaap.2014.10.006